Friction and Relaxation Dynamics of Highly Extended Polymer Brush Melts under Compression and Shear

Larisa Tsarkova,*,†,⊥ Xueyan Zhang,†,# Nikos Hadjichristidis,‡ and Jacob Klein*,†,§

Weizmann Institute of Science, Rehovot 76100, Israel; Department of Chemistry, University of Athens, Panepistimiopolis, Zografou, 157 71 Athens, Greece; and Physical & Theoretical Chemistry, University of Oxford, Oxford OX1 3QZ, UK

Received October 29, 2006; Revised Manuscript Received January 24, 2007

ABSTRACT: The forces between two adhering surfaces bearing highly extended polymer melt brushes as they are sheared past each other, and between a single melt-brush-bearing substrate sheared across an adhering bare solid surface, were studied using a mica surface force balance with a high shear-force resolution. The melt brushes were created by Langmuir−Blodgett deposition of zwitterion-terminated polyisoprene chains on the mica substrates. Shear of the single melt brush by the bare surface revealed little sliding, deformation, or relaxation of the confined melt brush, under all shear regimes applied in this study. In contrast, shearing of the two melt brushes past each other under the same shear conditions showed a marked shear-rate-dependent, multistage deformation of the sheared brushes. On stopping the applied lateral motion, a logarithmically slow relaxation of the stored stress was observed, which could be quantitatively interpreted in terms of mutual retraction of the entangled tails of the two brushes. The low friction and characteristic relaxation behavior following initial adhesive contact of the brushes developed with time to a solidlike response on shear of the confined chains and was attributed to bridging of chains adsorbed on the opposing surfaces as squeeze-out of the polymer occurred.

Introduction

Polymer brushes (polymer chains densely tethered onto a surface) have become a paradigm for modification of surface properties by polymers, and interactions between solid surfaces bearing such brushes have been extensively studied.[1] Experimental work over the past decade or so has also demonstrated that neutral polymer brushes can act as very effective lubricants between sliding surfaces immersed in a good solvent.[2−8] Most studies of the shear of polymer brushes to date have involved solvated brushes in a good solvent medium, with grafting density limited by the steric repulsion of the self-assembled brush chains, so-called "grafting-to". (Higher grafting densities can be achieved with grafting-from approaches, but these can result in quite high polydispersity[9] and moreover have not to date been grown on mica surfaces or used in friction studies.) The origin of the efficient lubrication in such cases, for example opposing polystyrene brushes in toluene (a good solvent), is attributed to the combination of large loads supported by the osmotic pressure of the compressed chains, together with the weak interpenetration of the two brushes arising from entropic factors. Up to moderate compressions this results in a fluid interface and hence low resistance to shear.[2,10] At much higher compressions—in the polystyrene/toluene case—a sharp rise in shear force was attributed to the rapid increase in the viscosity of polystyrene at high concentrations (approach to a glassy state).[4] However, in Θ solvents the onset of larger shear forces was found to occur at much lower compressions,[5,8] probably as a result of frictional dissipation occurring between the more readily interpenetrating tails.

* Corresponding author. E-mail: larisa.tsarkova@uni-bayreuth.de.
† Weizmann Institute of Science.
‡ University of Athens.
§ University of Oxford.
⊥ Present address: Physikalische Chemie II, Universität Bayreuth, 95440 Germany.
Present address: Newark College of Engineering, New Jersey Institute of Technology, University Heights, Newark, NJ 07102.

While the structure, normal forces, and shear behavior of solvated neutral polymer brushes are thus reasonably well understood, these ideas are unlikely to carry over well to melt brushes, i.e., brushes consisting of a melt of chains with no solvent, due to their specific space-filling constraints. In contrast to the repulsion of solvated brushes, melt-brush-covered surfaces, on approach in air, come into an adhesive contact[11] due to attractive van der Waals forces.[12] Consequently, they cannot stabilize surface interactions as can polymer brushes immersed in a good solvent.[13] On the contrary, tethered chains are used to enhance adhesion of coatings[14] and to modify surface wettability.[15] However, studying the dynamic response and the chain conformation as the solvent-free brushes are made to slide past each other is still a challenging problem. The dynamic experiments reported so far concerned systems that rather mimic real brush melts, ranging from polymer layer−silicate nanocomposites[16] and comb polymers[17] to macroscopic tooth brushes.[18] Theoretically, the rheology of grafted chains was first considered by Witten et al.,[19] who showed that there exists an interpenetration zone between two opposing (solvent-free) polymer brushes, and the thickness of this zone plays a major role in the rheology of the sheared grafted chains. Following their ideas, Joanny[20] examined the linear viscoelastic response of the melt brushes and considered the thinning of the interpenetration layer with the increase of the sliding velocity. Later, Semenov[21] ignored the entanglements inside the interpenetration layer and obtained a qualitatively different picture implying a smooth power like decrease of the effective viscosity. There have also been recent molecular dynamic simulations on brush dynamics, but to our knowledge these concern mainly solvated brushes[22,23] which do not interpenetrate unless strongly compressed together[4] and where solvent molecules contribute to the chains conformation by filling the voids between the chains.

In our previous paper[11] we reported a surface force balance (SFB) study on the adhesion and spontaneous thinning of a single polyisoprene-melt brush and of two mutually contacting

10.1021/ma062503g CCC: $37.00 © 2007 American Chemical Society
Published on Web 03/03/2007

polyisoprene brushes as well as on the stability of such melt brushes toward dewetting and cross-linking. Such highly stretched polymer monolayers created on mica via a Langmuir−Blodgett technique provide a good model of solvent-free brushes. The distinguishing features of these monodispersed brushes are the high grafting density and relatively high molecular weight, both resulting in high chain stretching. They also have the advantage of a well-characterized mean interanchor spacing and brush height, which can be deduced straightforwardly from the deposition procedure. The progressive extrusion of these brushes out of the confining gap could be satisfactorily described by a model based on the idea that the compressive elastic energy due to the adhesion was driving the chains to move laterally via the sliding of the zwitterionic anchoring groups along the surface. However, the time variation of the normal separation did not shed light on the differences between the different molecular organizations, in particular regarding the features of the interpenetration zone in the case of the two contacting melt brushes. To clarify this, we extend our investigation to focus mainly on the response to different patterns of applied *lateral* motions, which provide information also on molecular mechanisms of relaxation of the sheared brushes.

In this study we first recall briefly the main findings on the adhesion and spontaneous thinning of films consisting of a single brush and of a brush bilayer.[11] Then we discuss the behavior of these films in friction experiments using the SFB, both as single brush sheared against a bare mica surface, and particularly the case of opposing brushes in contact (i.e., bilayers) shearing past each other, as a function of time, extent of shear, and bilayer film thickness. In the final section we discuss the mechanism of the brush relaxation on cessation of the applied lateral shear motion, in terms of chain ends of one brush retracting from the entangled melt presented by the opposing brush.

Experimental Section

Materials. Linear polyisoprene (PI) end-terminated by the zwitterionic group $-(CH_3)_2N^+(CH_2)_3SO_3^-$ (henceforth −X: the zwitterion−mica sticking energy is ca. $8k_BT$[24]), with $M_w = 29\,900$ (designated PI−X) and near-monodisperse molecular weight distribution ($M_w/M_n = 1.06$), was used to prepare stretched brush monolayers. The polymerization procedure and structural details are described in ref 11. Dried samples of PI−X were stored in a deep freezer until use, avoiding direct contact with alcohols and water to minimize opportunities for hydrogen-bond complexation by the zwitterions. The polymer is a highly viscous clear liquid at room temperature (the glass transition temperature $T_g = -66$ °C).[25] It has an unperturbed radius of gyration $R_g = 0.8M_w^{1/2} = 137$ Å,[26] a bulk viscosity $\eta_0 = 9.38 \times 10^{-14}M_w^{3.66}$ P, entanglement molecular weight $M_{e,PI} = 5300$,[27] surface tension 31 mN/m, and density[28] $\rho_{PI} = 0.913$ g/cm^3.

Shear Force Measurements. The SFB used in the present study has been described in the preceding paper[11] and in more detail earlier, especially application of the shear motion and measurements of the shear force.[29] A brief description follows based on the schematic of the SFB in Figure 1.

The normal forces and lateral (or shear) forces $F_s(D)$ between two curved mica sheets, mounted in crossed cylinder geometry (mean radius of curvature $R \approx 1$ cm), are measured as a function of their separation by monitoring the bending of two orthogonal sets of leaf springs: vertical springs S_1 (spring constant $K_1 = 300$ N/m) and a horizontal spring S_2 (spring constant $K_2 = 150$ N/m). The bending of S_2 (on which the lower mica surface is mounted) is determined using multiple beam interferometry with an accuracy of about ±(2−3) Å. This is done by monitoring the change in wavelength of fringes of equal chromatic order (FECO) in response to the applied motion in the direction normal to the surfaces. The measured area S of flattened contact between the adhering surfaces may be used to evaluate the shear stress.

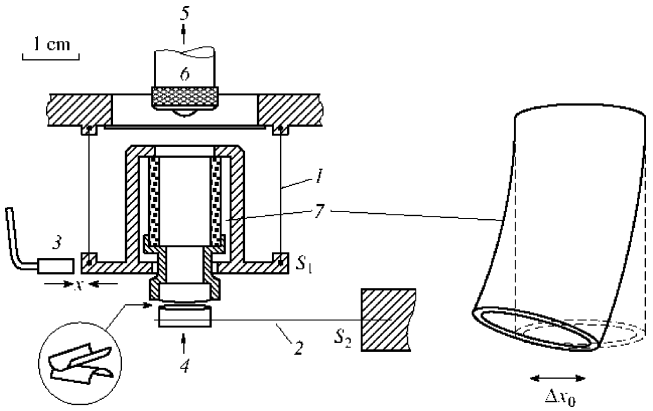

Figure 1. Schematic of the shear force balance (SFB[29]) used in the present experiments. The two mica sheets are mounted on cylindrical quartz lenses in a cross-cylinder configuration (inset). Heat filtered white light (4), passing through the SFB, undergoes interference in the gap between the back-silvered mica surfaces, and the wavelengths are transmitted to a spectroscope (5) through the microscope tube (6). The closest distance D between the surfaces is measured to ±(2−3) Å using multiple beam interferometry. The top lens is mounted on a sectored piezoelectric tube (7), which can apply both normal and lateral motion to the top mica surface. Normal forces are measured via the bending of the horizontal stainless steel leaf spring S_2 (2) (spring constant K_2). Shear forces are measured via bending of the shear force springs S_1 (1) (spring constant K_1), monitored by capacitance changes of an air gap x via the capacitor probe (3).

The top mica surface is mounted on a sectored piezoelectric tube (PZT), which can provide smooth controlled motion in directions normal and parallel to the surfaces. The bending of S_1 in response to the shear forces is detected by the changes in the capacitance of a small air gap x whose variation (Δx) derives from the bending of the shear springs S_1 (Figure 1). The capacitance bridge (Accumeasure 5000, probe ASP-1-ILA, MTI Ltd., Albany, NY) enables high sensitivity in measuring shear forces F_s directly up to ca. ±0.1 μN via the relation $\Delta F_s = K_1\Delta x$.[29]

In a shear experiment, in addition to measuring the surface separation D, two outputs are recorded simultaneously using a storage oscilloscope (LeCroy 9304A). These are the voltage applied to opposing sectors of the PZT, which gives a direct measure of the applied lateral motion Δx_0, and the signal from the capacitor bridge, which monitors the bending Δx of the vertical springs S_1 and thereby provides a direct measure both of the shear force F_s ($=K_1\Delta x$) and of the extent of sliding $\Delta x_{sl} = \Delta x_0 - \Delta x$. Two patterns of applied motion were used in the present study: In the first, following a period of rest, a steady lateral motion was applied for a given time and at a given velocity v_s, followed by a relaxation period when the applied lateral motion was stopped; in the second, a back-and-forth lateral motion (triangular function) was employed. We also briefly note shear responses to an applied sinusoidal motion.

Experimental Procedure. In every experiment the air-contact position between bare mica surfaces was calibrated (by noting the corresponding FECO wavelengths) prior to the deposition of the monolayers. The lenses were then taken out of the SFB and fixed in the lens holders of the Langmuir−Blodgett minitrough (KSV, Finland), the deposition was carried out, and the lenses were mounted back in the apparatus (all done in the laminar flow hood). The deposition procedure and the variation of the surface pressure vs area per molecule isotherm of the PI−X monolayer on water substrate are described in refs 11 and 30. Prior to measurements the polymer layers were dried inside the box under filtered, dry nitrogen flow for several hours. Following approach of the surfaces and their jump into adhesive contact, the changes in the film thickness D as well as changes in the shear forces in response to the applied shear pattern were continuously monitored. No external compression was applied to the surfaces following their jump into

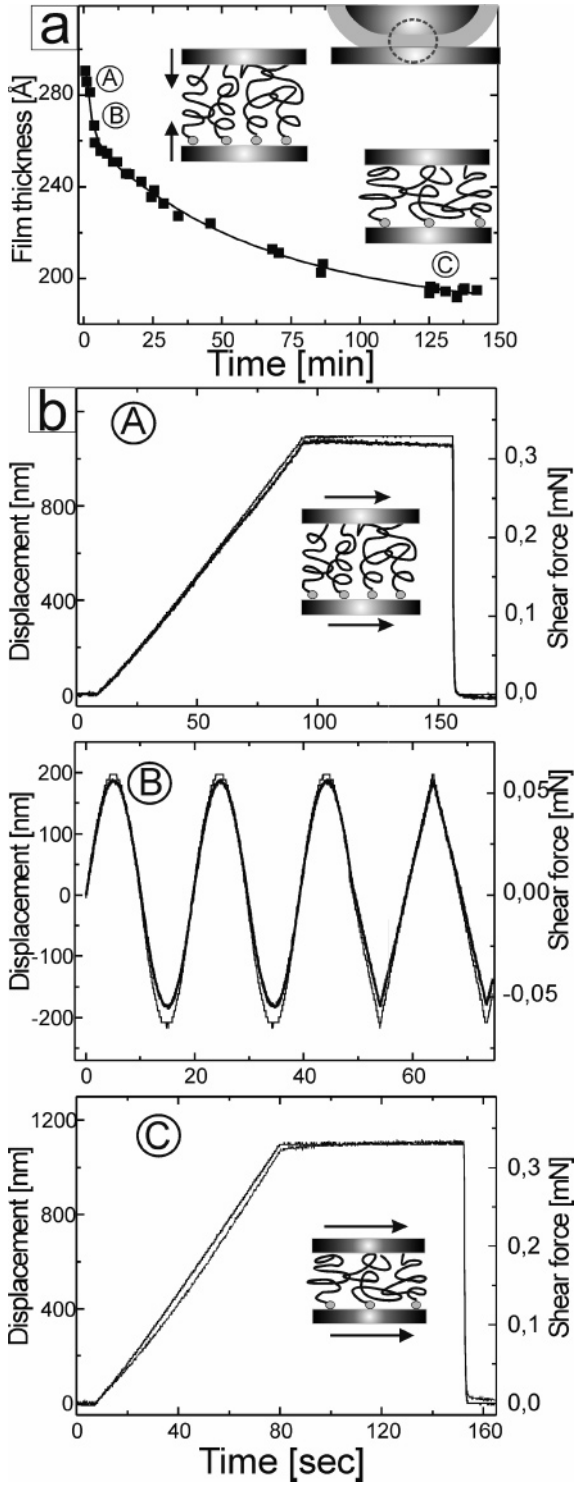

Figure 2. (a) Kinetics of thinning of the PI−X monolayer following the jump in to adhesive contact. The solid line through the symbols is the fit with an exponential decay (adapted from ref 11). The cartoons suggest possible configurations of the brush monolayer following the jump in (left cartoon) and at the end of the measurements (right cartoon), indicating the increase in mean anchor spacing as chains are extruded out at the later time (RH cartoon). The letters indicate the time and the monolayer thickness at which corresponding shear responses shown in (b) have been monitored. (b) The shear traces of the PI−X monolayer at different applied shear modes (a linear motion followed by a stopping period as in A and C or sinusoidal/triangular as in B). The data are plotted as the applied displacement to the top surface Δx_0 (thin line) and the actual displacement of the lower surface Δx (bold line). The RH axis gives the corresponding shear forces. All shear responses shown are characteristic of a solidlike behavior, where the applied lateral motion of the top surface and the response of the lower surface are almost identical (i.e., little sliding ($\Delta x_0 - \Delta x$) of the surfaces).

contact. The radius of the flat contact area a was measured directly from the fringe shape and was generally in the range 15−25 μm. Shear results shown here are from four different experiments, with data taken from a number of different contact positions in each experiment. All measurements were carried out in a dry nitrogen atmosphere.

Results and Discussion

Normal Interactions and Spontaneous Thinning. In both the case of two opposing PI−X brushes, or that of a single brush facing bare mica, the surfaces jumped into an adhesive contact on approach, driven by van der Waals forces, and the films started to thin spontaneously, as earlier described and as reproduced in Figures 2a and 3a for the PI−X monolayer and bilayer, respectively. The applied lateral movement consisted of the initial rest period and then steady applied motion followed by a cessation of applied motion for a further period. The top surface was moved laterally at velocity $v_s = dx_0/dt = 15$ nm/s over a distance of about 1.2 μm, which considerably exceeds the thickness D of the sheared polymer films. For an applied motion of the top surface $\Delta x_0 = v_s t$, the surfaces slide past each other by an amount $\Delta x_{sl} = \Delta x_0 - \Delta x$, where Δx is the amount by which the lateral springs bend (revealed by the output of the capacitance bridge). The measured shear force at any point is given by $\Delta F_s = K_1 \Delta x$.

The extent and variation with time of the deformation of the confined brush melt layers, the sliding of the surfaces, and the shear forces between them are conveniently shown by plotting the applied lateral motion Δx_0 and the spring bending Δx as a function of time. This is illustrated for the PI−X monolayer and bilayer in Figures 2b and 3b, respectively, for different applied shear patterns at progressive elapsed times from contact (corresponding to different thickness of the confined brushes). While the normal separations showed similar behavior for monolayer and bilayer architectures, the shear responses following the jump-in to contact were strikingly different.

Single PI−X Monolayer Trapped between Mica Surfaces. In the case of a monolayer, the shear response was always largely solidlike in the sense that there was little shear deformation of the confined films under the range of shear conditions applied in the present study. Within the range of our accessible parameters, this solidlike behavior held for different forms of the applied shear motion (linear lateral motion as in Figure 2b(A and C) or periodic sinusoidal (or triangular) as in Figure 2b(B)) and at different times following the jump-in to contact, that is, at different extents of extrusion of the layer. In other words, at the applied lateral velocities and shear amplitudes of the top confining surface, and over the time scales of the measurements, the shear force across the molten brush monolayer was insufficient to cause significant shear deformation or to lead to sliding between the two confining surfaces. For the sinusoidal motion, left-hand side of Figure 2b(B), a very small phase shift may be discerned between the applied shear motion Δx_0 and the shear force across the film, $F_s = K_1 \Delta x$. (The stress across the film is related to the shear force F_s, while the small difference between Δx_0 and Δx is related to the strain across the film.) In principle, such small-strain data can be used to extract information on the linear viscoelastic properties of the sheared film. However, in the present work we are interested primarily in molecular relaxation effects more closely related to large-scale sliding of the surfaces past each other. For these reasons we will not pursue this further here.

The above result indicates that little shear or sliding at the interface between the brush ends or the zwitterionic head groups and the respective mica surfaces occurs under the shear regimes

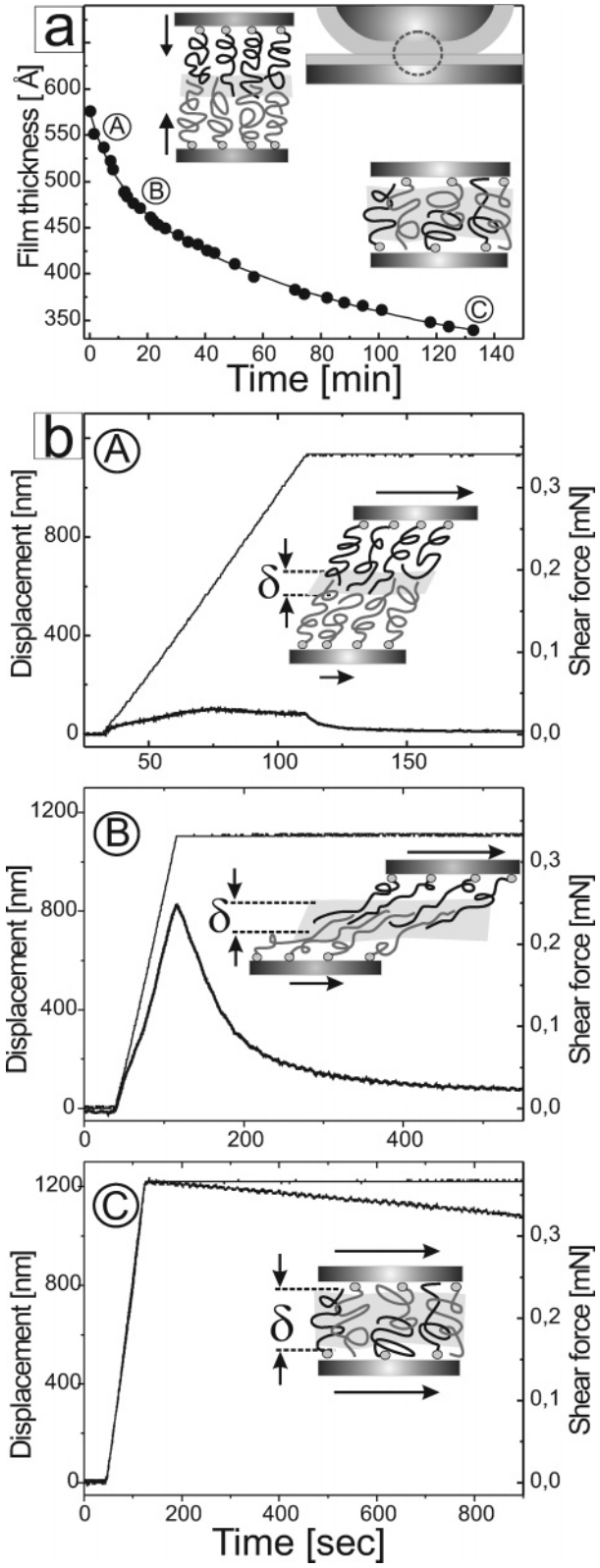

Figure 3. (a) Kinetics of thinning of the PIX brush bilayer following the jump in to adhesive contact, fitted by the exponential decay (solid line) (adapted from ref 11). The cartoons indicate the proposed configuration of the brush bilayer shortly after the jump-in (left cartoon) and at the end of the measurements (right cartoon; note increase in mean brush−anchor spacing). (b) The lateral motion applied to the upper surface (upper trace, LH axis) and transmitted shear force (lower trace, RH axis) at the points of the time/thickness indicated by corresponding letters in (a). (A) Motion between opposing PI−X brushes following the jump-in proceeds with low friction. The shear force across the bilayer increases with decreasing film thickness (B) until a quasi-solid-like behavior is reached (C).

applied in these experiments. The only discernible stress relaxation in the sheared brush monolayer was observed after the cessation of the shear when it was applied shortly after the jump-in, as seen in Figure 2b(A) in the very slight decrease in the shear force. At later stages of the film thinning this kind of relaxation vanished (Figure 2b(C)).

It is of interest to estimate the behavior if the confined PI melt layer were to relax with a viscosity η_{PI} characteristic of the bulk. We could then estimate the resulting shear force across the surfaces as follows: For a PI melt film of thickness $D \sim 2R_g$ and an area equal to the flat contact area S between the two surfaces, sliding past each other with velocity v, the shear force F is given by the standard equation for Couette flow:[31]

$$F = S\eta_{PI}v/D \quad (1)$$

Substituting for the viscosity of bulk PI (η_{PI} = 230 Pa·s) and the applied shear velocity given by the slope $d(\Delta x_0)/dt$, we find $F \approx 0.05$ μN. This is some 4 orders of magnitude lower than the maximum shear force sustained by the confined PI−X monolayer in our experiments, and even such a large force does not lead to the deformation of the confined film. The underlying reason for this is the fact that every chain in the confined single brush layer is attached by its zwitterionic end group to one confining mica surface, while in the case of many—if not all—of the chains they are further adsorbed strongly on the opposing mica surface. This attachment prevents chains leaving the surface over extended times and results in a strong suppression of the molecular relaxation pathways that are available in an unconstrained bulk sheared polymer melt. It thus leads to the solidlike behavior observed. This simultaneous attachment to both surfaces by the chains in the gap is also the reason why the viscoelastic properties of the sheared, confined monobrush would be difficult to interpret in terms of the standard approaches applied to polymer melts.

Shear of Two Opposing Melt Brushes: General Features. In contrast to the solidlike behavior of a single brush, the response on shearing two contacting, melt-brush-bearing surfaces under the same conditions exhibited a wide range of relaxation behavior, as shown in Figure 3. For an applied shear pattern similar to that in Figure 2, that is, a rest period, followed by uniform applied lateral motion of one of the surfaces for a period and then cessation of the applied motion, there are three broad patterns of relaxation, as shown in Figure 3b(A, B, C), depending in turn on the extent of extrusion of the brushes from between the confining surfaces. Shortly after the jump-in to contact, Figure 3b(A) corresponding to point A in Figure 3a, the shear force rises initially with some sliding, then (following a maximum) reaches a plateau where the surfaces slide freely past each other, and finally, on cessation of the applied lateral motion, relaxes slowly. At intermediate times of extrusion (Figure 3b(B) and point B in Figure 3a), the shear force rises (with some sliding), but a free-sliding plateau is not attained prior to cessation of the applied shear, following which the shear force across the films again relaxes slowly. Finally, following substantial extrusion, when the surface separation D approaches 300 Å, Figure 3b(C) (point C in Figure 3a), the shear force rises sharply on first applying the shear motion, with essentially no sliding, and some slow relaxation is observed following cessation of the shear. It is of interest that this value of D, where the melt brush bilayer is almost solidlike, is similar to the thickness of the PI−X monobrush on initial contact with the opposing mica surface, where a similar solidlike behavior is observed (Figure 2b(A)).

A further telling difference in the shear behavior of a monolayer and a bilayer configurations was revealed while applying a sinusoidal shear. The shear response of a single brush melt produced a sinusoidal shear force response almost exactly in phase with the drive independent of the time in contact (see Figure 2b(B)). In contrast, shortly after the jump-in of the two brush covered surfaces, the shear response (not shown) was some 25° out of phase with the drive. This points to the much greater scope for relaxation of the sheared bilayer in initial contact, though our discussion here focuses mainly on effects related to larger scale sliding of two brush-covered surfaces.

Although SFB measurements do not provide direct access to the molecular configurations in the polymer film, the difference in behavior at progressive times (Figure 3b, A ⟹ B ⟹ C) shows clearly that the conformational changes occurring during the adhesive contact have a significant effect on the viscoelastic response of the system. The increase of the frictional response of the brush bilayer system is attributed to the increasing extent of interdigitation arising from the increase in chain spacing (i.e., decrease in surface density of chains) as the brushes extrude and is illustrated in the respective cartoons in Figure 3. Another scenario of the structure evolution as the chains are extruded is the fluctuation-induced interfacial roughening between rubbing brushes, as was recently proposed for sheared brushes between the limits of good and theta conditions.[8] Resulting from this scenario, the opposing chains are mutually compressed and either interlock or entangle with a chain from the opposing surface. Additionally, because of the reduced grafting density arising from the extrusion, the tethered chains reconfigure to fill space at the mica surface where the zwitterionic attachment point is located. This adsorption is important, as it prevents a slip plane from locating at the mica−brush interface and dominating the frictional response of the system. We attribute the onset of solidlike behavior in Figure 3b(C) to the extent that adsorptive bridging of the brush chains attached to the opposing surfaces occurs. This in turn is manifested in the suppression of relaxation pathways over the times of our experiments, similar to that discussed for the brush melt monolayer above.

We note that the complex structure of the melt-brush-covered surfaces reported here, as well as the spontaneous adhesion between them, suggests that it would not be meaningful to compare our results with the behavior of solvated polymer brushes[2,4,6,8] or adsorbed polymer layers,[7,32] where repulsive interactions dominate the friction behavior.

Shear of Weakly Interpenetrating Opposing Melt Brushes. The difference in shear responses in Figures 2b and 3b is especially striking immediately following the jump-in, when we believe the stretched configuration of each as-deposited melt brush is preserved and the opposing brushes are only slightly interdigitated. We now focus on this type of response, as shown in Figure 4 (similar to that in Figure 3b,A) for contacting melt brush bilayers, progressively thinning though still in the weak interpenetration regime.

Several characteristic regimes can be clearly identified in this set of shear responses. For a short period following the commencement of uniform, lateral motion of the top mica surface at time $t = 0$, little sliding between the surfaces occurs (Figure 4, region A−B), and the shear force increases as most of the applied lateral motion is taken up by bending of the shear springs. On increasing shear, the surfaces start to slide past each other: at around the point B sliding is first clearly noted, and further applied lateral motion of the top surface (from B onward) is taken up in part by sliding between the surfaces and the rest by bending of the shear springs.

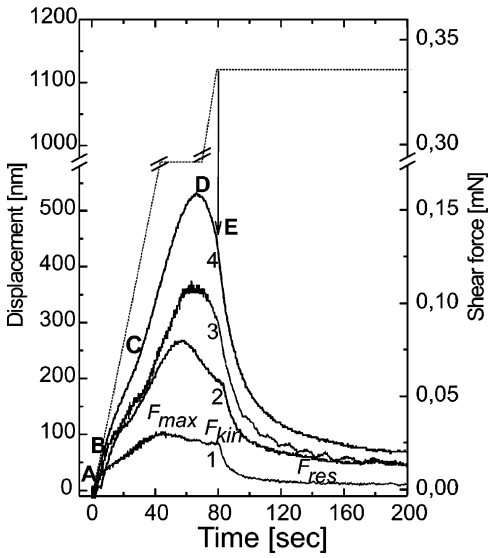

Figure 4. (a) Typical shear responses for the PI−X brush-covered mica surfaces showing the displacements of the input and output shear signals (LH axis) and the evolution of the shear force with time (RH axis) while applying the ramp driving function with a lateral shear velocity 15 nm/s. The dotted line is the motion applied to the top mica surface, and the lower traces show the displacement of the lower mica surface (LH axis) and shear forces across the bilayers (RH axis) corresponding to different bilayer film thickness. From bottom to top: traces 1: 460 ± 15 Å; 2: 430 ± 10 Å; 3: 420 ± 7 Å; 4: 380 ± 5 Å. The arrow points to the stop of the applied motion (end of the ramp shown by the dotted line). Letters indicate transitions to different regimes in shear responses. Parameters of shear responses are summarized in Table 1.

At around the point C (whose position shifts to larger shear-stress values as the films thin) a characteristic point of inflection in the increase of $F_s(t)$ is observed. At this point the surfaces slide rather faster past each other for a short period and then slower again: it is reminiscent of stick−slip in solid−solid friction,[33] though much less marked and emanating from a very different mechanism at the molecular level.[6] Following this, while the top surface is still moving laterally, a maximum F_{max} in $F_s(t)$ is attained (point D), following which the shear force decreases, either to a clearly marked plateau value (kinetic friction) for the shortest extrusion times (trace 1) or to a lower value when the applied lateral motion ceases (arrow). Such a plateau (seen most clearly in trace 1 of Figure 4 and also in trace b(B) of Figure 3), where the shear force is equal to the kinetic friction F_{kin}, corresponds to steady sliding of the surfaces past each other. Similar plateaus (though arising from different molecular mechanisms) were observed in shear of short polymer melts,[34] dendrimer monolayers,[35] and—in a configuration similar to the present one—across compressed brushes in a good solvent.[4,6] The reason why similar plateaus are not clearly seen for the longer extrusion time brushes (curves 2−4) is due, we believe, to the limited lateral motion we were able to apply via the PZ tube. Thus, the applied lateral motion ceased (arrow in Figure 4) before a free-sliding plateau could be attained. We note that the value of F_{max} increases as the bilayer thins, as does the time t_{max} required to reach F_{max}. Finally, following the cessation of the applied lateral motion (point E), the shear force decays in a characteristic fashion, which we consider in detail in a subsequent section (and in Figure 7 later).

In Table 1 we summarize the following characteristic parameters for each of the curves from Figure 4: the maximum shear force F_{max} across the film at t_{max}, the extent by which the surfaces have slid past each other when F_{max} is attained (given

Table 1. Characteristic Parameters of Shear Responses (as in Figure 4)

Fig 4 trace	D, Å	t_{max}, s	F_{max}, μN	Δx_{slide}, nm	F_{kin}, μN	τ_1, s	F_{res}, μN, (after 200 s)
1	460 ± 15	44	30	500	25	6.1	3
2	430 ± 10	53	78	470	~45	6.9	13
3	420 ± 7	59	105	470		8.2	13
4	380 ± 5	68	160	430		10.7	21

by $\Delta x_{slide} = \Delta x_0 - \Delta x$); the value of the kinetic friction F_{kin} at the sliding plateau (where this could be measured or extracted); the characteristic relaxation time upon the cessation of the shear τ_{rel}; and the residual shear force F_{res} following 200 s of relaxation subsequent to cessation of the applied shear motion.

We remark finally that the sliding friction coefficient μ_{eff} for the initial contact (trace 1) may be estimated from the effective overall load and the shear force at sliding ($F_{kin} \approx 25$ μN, from trace 1 in Figure 4). Although no external load is applied, as described in ref 11 the adhesion between the surfaces is equivalent to a compressive load $F_{comp} \approx 4.6\gamma_{PI}R$, where γ_{PI} is the surface tension of the PI melt and R the undeformed radius of curvature (≈1 cm). This gives $F_{comp} \approx 1.4$ mN. Thus, $\mu_{eff} = F_{kin}/F_{comp} \approx 25$ μN/1.4 mN ≈ 0.02, a relatively low value.

Shear Rate Dependence of the Shear Force. The shear response of rubbing brushes at varying shear rates is of interest as it is related to the understanding of molecular friction and has been a subject of several theoretical studies. Most of these dealt with solvated brushes, addressed the steady-state regime, and found a decrease in the effective viscosity with the increasing shear rate[23] (shear thinning).

For the interpenetrated polymer melt brushes in our system, we examined qualitatively the effect of increasing shear rate on the shear force, for a given bilayer thickness. The top mica surface confining the bilayer was subjected to back-and-forth motion (triangular pattern, top trace) at fixed shear amplitude ($\Delta x_0 = \pm 450$ Å) but at increasing driving frequency, and the corresponding shear force vs time traces for a 460 ± 10 Å thick PI−X bilayer are shown in Figure 5. The data are qualitative insofar as a flat plateau in the shear force vs time traces (which would yield the kinetic friction or equivalently the effective viscosity of the interpenetration zone) is not reached even for the lowest drive frequency (0.01 Hz). At the same time there is clear "hardening" of the response at the higher drive frequencies, with little sliding being detected above 1 Hz, signaling onset of a solidlike response. This indicates that the corresponding shear rates exceed the accessible relaxation rates of the interpenetrated chains. In molecular terms, it implies that the interpenetrated chains being pulled laterally have little scope for stretching, as the entangling network surrounding them undergoes little relaxation in the available time (<1 s).

Shear Response on Decompression. In our earlier paper[11] we described measurements of the pull-off forces of molten PI−X brushes which were carried out to probe the viscoelastic adhesion mechanisms in these polymer films. These experiments revealed pull-off rate-dependent interactions of the mutually interpenetrated brush melt layers and the rupture of the brush layers following the jump-out. Here we focus on the shear response of the bilayer brush melts when they are subjected to a tensile force in adhesive contact.

As noted, following progressive extrusion after the jump-in to contact, the shear response becomes increasingly more solidlike, and any relaxation becomes more sluggish. In Figure 6 we show the effects of applying a tensile force on the shear response of the adhering brush bilayer. Such a tensile force may be viewed as a decompression load and may be applied by

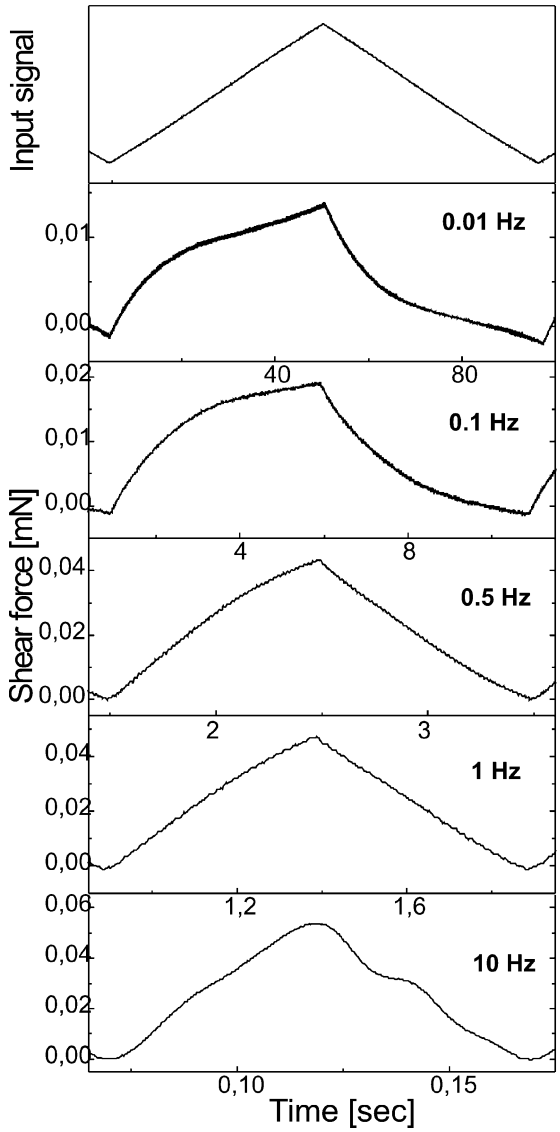

Figure 5. (a) Shear force vs time traces across PI−X brushes in contact (bilayer thickness 460 Å) as a function of the frequency of the lateral back-and-forth motion applied to the upper surface (upper trace) with constant shear amplitude Δx_0 (±450 Å). Note that the scale of the force axes increases at higher frequencies, so that the highest shear force attained over a cycle (for the given shear amplitude we apply) increases up to ca. 1 Hz where it saturates.

contracting the piezoelectric tube on which the top surface is mounted. Trace 1 of Figure 6 shows the lateral motion pattern applied to the top mica surface, while traces 2−4 show the corresponding shear force between the adhered bilayers. Trace 2 shows the response prior to application of a decompressive load, revealing an almost solidlike response following significant extrusion as described earlier (Figure 3). Traces 3 and 4 show the shear forces on gradually contracting the piezoelectric tube (PZT) to apply a progressively increasing tensile force as noted above. We see that application even of a small extent of decompression results in some recovery of the relaxation rate (and also of the phase shift in the sinusoidal shear response, not shown here). As clearly seen in traces 3 and 4 compared with trace 2, both the extent of sliding between the sheared surfaces during the applied lateral motion and the relaxation rate upon the cessation of shear are considerably enhanced by the decompression. We emphasize that the actual change in contact area S due to the decompression leading to traces 3 and 4 is smaller than our detection limit (within 5−10%), while the

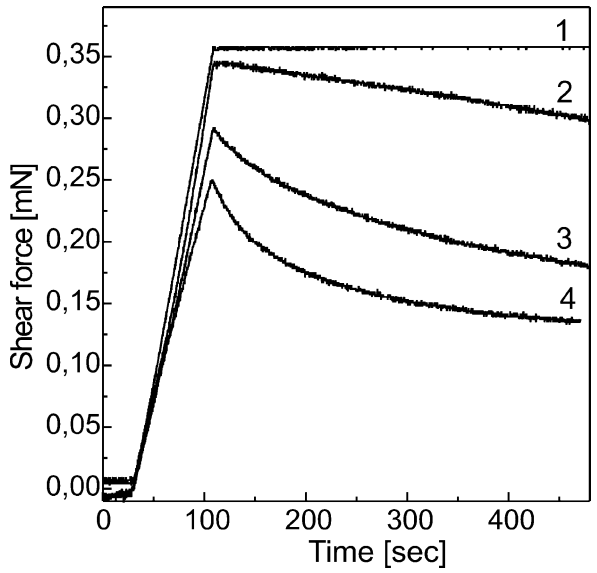

Figure 6. Shear behavior upon applying a decompression load to the brush bilayer in contact. Directly recorded shear traces: (1) applied shear motion to upper surface; (2) shear force across the brush bilayer in a solidlike regime (about 130 min in contact), prior to application of decompression; (3, 4) shear responses of the same bilayer as in trace 2, but under a weak decompression (trace 3) and a slightly larger decompression (trace 4), as described in the text.

value of the bilayer thickness also does not noticeably change as a result of the decompression. Thus, the changes in the relaxation and sliding behavior are likely due to structural changes within the bilayer itself. We attribute this to the tensile stress causing some desorption of bridging chains from opposing brushes, on the one hand, and possibly to some disentanglement of chains from the interpenetration zone, on the other. Importantly, shear traces of a single PI−X monolayer under similar shear tests did not show any signs of the enhanced relaxation, which indeed would not be expected on the basis of the above mechanism (since the total number of bridging chains for a monolayer is a function only of the contact area and surface density of chains).

Mechanism of the Brush Shear and Relaxation. A central finding of this work concerns the frictional force and its relaxation following shear of the rubbing melt brushes, as revealed particularly in the data of Figure 4. The essential picture is one where the two melt brushes interact and interpenetrate on contact. Upon shear, the mutually interpenetrated chains are both stretched and also pulled out of the interpenetration zone, as indicated in the cartoons in Figure 3b.

Examining in more detail trace 1 of Figure 4, where the main features are most clearly marked, we note the initial rapid rise in the shear force corresponding to the stretching of the chain moieties in the interpenetration zone. This is followed by a maximum (F_{max}) which is the shear force when the increasing chain tension is just balanced by the drag on it within the interpenetration zone as the chains are pulled out and subsequently by a spontaneous decrease in this maximum as the additional tension causes the chain ends to be pulled out faster than the mutual sliding velocity of the surfaces. This has been interpreted[6] as a sort of "stick−slip" event, though it has a different molecular origin than in friction between solid surfaces and has also been conjectured earlier.[20]

We also remark on the increasing magnitude of F_{max} with the thinning of the brush bilayer, on going from trace 1 to 4 (in Figure 4). This occurs because as the melt bilayer extrudes and thins, we expect also greater interpenetration of the brushes. Thus, longer portions of the chains—the interpenetrated portions—are stretched upon shear, and F_{max} increases. The cartoons in Figures 3b(A) and 3b(B) respectively illustrate the behavior at lesser and greater interpenetration.

While this is to our knowledge the first experimental study of melt brush interaction and shear, similar shear experiments have been carried out by Tadmor et al.[6] where two self-assembled solvated brushes in a good solvent were compressed to around 70% volume fraction of polymer and then sheared. This earlier study differs from the present polymer melt one in the grafting density and in some effect of the solvent, while in the current study the progressive extrusion of the contacting melt brush bilayer provided an additional variable which varied the frictional forces on shear. Nonetheless, the analysis applied there—to shear of compressed, high density, entangled brushes well above their glass transition—should also hold in the present system. Thus, we may examine the stress relaxation in the brush melt (in traces in Figure 4) in light of the analysis in ref 6.

Stress relaxation after the applied motion was ceased is initially rapid but then becomes logarithmically slow (Figure 4). This has been interpreted quantitatively in terms of an "arm-retraction" mechanism[6] where the chains from each brush relax by retracting from their entanglements within the mutual interpenetration zone. We now examine this logarithmic relaxation mode in more detail. According to the model presented earlier,[6] the measured shear force $F_s(t)$ decays with time as the residual stress is borne by the remaining unrelaxed portion of the interpenetrating chains, according to[6,36]

$$[F_s(0) - F_s(t)]/F_s(0) \cong (l_e/\alpha L_0) \ln[t/\tau] \quad (t \geq \tau) \qquad (2)$$

Here $F_s(0)$ is the tension when the chain retraction commences (corresponding in our experiments to the point E in Figure 4), l_e is the polymer entanglement length, L_0 is the fully stretched end-to-end length of the polymer (its total contour length), and $\alpha \approx 0.6$ is a constant. τ is a characteristic time related to the reptation time of the interpenetrated portion of the brushes and of magnitude of order 1 s or less for the present system. In Figure 7 we plot $[F_s(0) - F_s(t)]/F_s(0)$ vs $\ln(t)$ from the shear traces in the relaxation region indicated by arrows in RH insets to Figure 7. The brush responses following the jump in (curves 1 and 2) are compared to the brush behavior at later time (curves 3 and 5) and to the brush relaxation upon application of decompression load. The linear fit of curves 1 and 2, which correspond to the upper and lower traces of Figure 4, as well as of curve 3 gives a slope 0.28 ± 0.02. The onset time in the $\ln(t)$ axis (a few seconds) may possibly be attributed to the fact that, except for curve 1, in all the other shear response traces the applied motion was stopped before the steady-state sliding was fully reached. At higher degree of brush interpenetration (curve 5) as well as in decompressed brushes (curve 4) the slopes deviate from the above value, indicating other relaxation pathways.

According to the model, the magnitude of the logarithmic slope ($l_e/\alpha L_0$), from eq 2, should be related to the total number of entanglement lengths (L_0/l_e) = (M/M_e) and is predicted for the PI−X brushes to be close to 0.3 ($M_e/\alpha M = 5.3 \times 10^3/(0.6 \times 29 \times 10^3) = 0.3$). The closeness of agreement between the predicted (0.3) and experimentally measured (0.28 ± 0.2) slopes is unlikely to be fortuitous even in view of the approximations[6] leading to eq 2. It is especially interesting to compare these predicted and observed values to those in ref 6, where a different polymer, a zwitterion-terminated poly(ethylene propylene), designated PEP−X, was used for the brush (and a correction made for the volume fraction of monomers in the highly

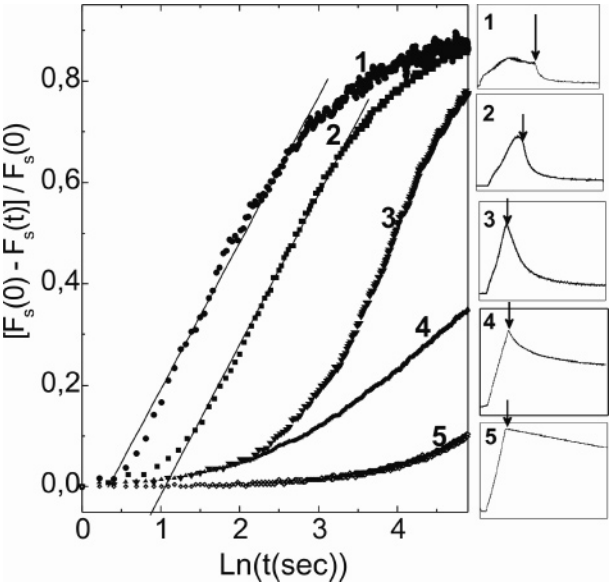

Figure 7. Relaxation regime at time t after the cessation of the applied motion plotted as $[F_s(0) - F_s(t)]/F_s(0)$ vs $\ln(t)$, where $F_s(0)$ is the value of the shear force at the point indicated by an arrow in each shear trace shown in the panels on the right side (trace numbers correspond to curve numbers in the main figure). The straight lines in curves 1 and 2 have a slope 0.28. Curves 1 and 2 correspond to traces 1 and 4 in Figure 4; curves 3 and 5 correspond to shear traces in Figures 3b-(B) and 3b(C), respectively. Curve 4 corresponds to trace 4 in Figure 6.

compressed solvated brushes). For the polymer parameters in the PEP−X brush study,[6] the predicted value of the slope was 0.04 while the experimental fit gave a slope 0.038. Thus, although the predicted value of the slope in the present study differs by almost an order of magnitude from that in the earlier work, the experimental values in both cases are very close to the respective predictions. This provides strong support for the idea that the molten brushes do indeed relax in a manner similar to an array of dangling ends in an entangled matrix, which is the essence of the model leading to eq 3. In the present work we see this agreement of predicted vs observed slope over a wide dynamic range and for different bilayer thicknesses corresponding to different extents of extrusion of the brushes (different traces in Figure 4), indicating that the model is robust.

Summary and Conclusions

A surface force balance was used for the first time to probe the shear behavior of highly stretched polymer brush melts well above their glass transition temperature. Within the range of our applied shear, the response of a single PI−X monolayer trapped between mica surfaces is solidlike; i.e., it can sustain a shear stress almost with no relaxation for extended periods. This is presumably due to the strong zwitterionic tethering of the chains on one surface together with their substantial adhesive interactions with the opposing surface. These two constraints must block relaxation pathways by trapping the chains and their mutual entanglements for the extended periods associated with overcoming the attachment to the substrates.

In contrast, when two polymer melt brushes are brought into contact to form a bilayer, and made to slide past each other, the shear behavior is very different from the single brush case, suggesting that the sliding takes place rather in the interfacial plane between the brushes. In friction experiments at low shear rates the output signal is primarily determined by the thickness of the brush bilayer or equivalently by the width of the interpenetration zone. These can be varied by making observations at different extents of extrusion of the bilayer. The lateral force between weakly interpenetrating brushes (low extent of extrusion) as the shear motion grows shows a characteristic maximum in the shear force, attributed to initial stretching of the interpenetrated chains, followed by spontaneous relaxation to the steady-sliding regime as chains relax away from their stretched configuration. Kinetic sliding of the surfaces initially proceeds with relatively low friction (friction coefficient $\mu \sim 0.02$) under the adhesive load between the contacting brushes. As the melt bilayers undergo progressive extrusion and consequent thinning, the lateral force in response to shear remains qualitatively similar to that on initial contact, but at a higher magnitude of force, reflecting the greater interpenetration as the layers extrude.

While the above observations are largely qualitative, a telling point is noted when, following shear at relatively weak interpenetration, the applied sliding motion is stopped. The residual shear stress is then observed to decays logarithmically over a significant dynamic range, at a rate quantitatively very close to that predicted for the relaxation of an entangled network of dangling PI−X chains in a melt. These predicted values differed by about an order of magnitude from the logarithmic relaxation rate predicted in an earlier study for a rather different polymer system (compressed PEP−X brushes). The fact that in both experiments the observed logarithmic relaxation rates were very close to the (widely differing) respective predictions suggests that the model of "dangling-end" relaxation represents well the molecular mechanism of interactions between the compressed, sliding brushes.

Acknowledgment. We thank the Israel Science Foundation for their support of this work. L.T. acknowledges the support of the State of Bavaria (HWP Program).

References and Notes

(1) Milner, S. T. *Science* **1991**, *251*, 905−914. Halperin, A.; Tirrell, M.; Lodge, T. P. *Adv. Polym. Sci.* **1992**, *100*, 31−71. Grest, G. S. *Adv. Polym. Sci.* **1999**, *138*, 149−183.
(2) Klein, J. *Annu. Rev. Mater. Sci.* **1996**, *26*, 581−612.
(3) Klein, J.; Kumacheva, E.; Perahia, D.; Mahalu, D.; Warburg, S. *Faraday Discuss.* **1994**, *98*, 173−188. Drobek, T.; Spencer, N. D.; Heuberger, M. *Macromolecules* **2005**, *38*, 5254−5259.
(4) Klein, J.; Kumacheva, E.; Perahia, D.; Fetters, L. J. *Acta Polym.* **1998**, *49*, 617−625.
(5) Schorr, P. A.; Kwan, T. C. B.; Kilbey, S. M., II.; Shaqfeh, E. S. G.; Tirrell, M. *Macromolecules* **2003**, *36*, 389−398.
(6) Tadmor, R.; Janik, J.; Klein, J.; Fetters, L. J. *Phys. Rev. Lett.* **2003**, *91*, 115503.
(7) Raviv, U.; Frey, J.; Sak, R.; Laurat, P.; Tadmor, R.; Klein, J. *Langmuir* **2002**, *18*, 7482−7495.
(8) Forster, A. M.; Mays, J. W.; Kilbey, S. M., II. *J. Polym. Sci., Part B* **2005**, *44*, 649−655.
(9) Ruths, M.; Johannsmann, D.; Ruehe, J.; Knoll, W. *Macromolecules* **2000**, *33*, 3860−3870.
(10) Klein, J.; Kumacheva, E.; Mahalu, D.; Perahla, D.; Fetters, L. J. *Nature (London)* **1994**, *370*, 634−636.
(11) Tsarkova, L.; Zhang, X.; Klein, J.; Hadjichristidis, N. *Macromolecules* **2002**, *35*, 2817−2826.
(12) Tadmor, R. *J. Phys.: Condens. Matter* **2001**, *13*, L195−L202.
(13) Fleer, G. J.; Cohen-Stuart, M. A.; Scheutjens, J. M. H. M.; Cosgrove, T.; Vincent, B. *Polymers at Interfaces*; Chapman and Hall: London, 1993. Napper, H. D. *Steric Stabilization of Colloidal Dispersions*; Academic: London, 1983.
(14) Sides, S. W.; Grest, G. S.; Stevens, M. J.; Plimpton, S. J. *J. Polym. Sci., Part B* **2004**, *42*, 199−208.
(15) Yerushalmi-Rozen, R.; Klein, J.; Fetters, L. J. *Science* **1994**, *263*, 793−795. Long, D.; Ajdari, A.; Leibler, L. *Langmuir* **1996**, *12*, 1675−1680.
(16) Krishnamoorti, R.; Giannelis, E. P. *Langmuir* **2001**, *17*, 1448−1452.
(17) Bailly, C.; Stephenne, V.; Muchtar, Z.; Schappacher, M.; Deffieux, A. *J. Rheol.* **2003**, *47*, 821−827.
(18) Kotomin, S. V.; Avdeev, N. N. *Wear* **1998**, *222*, 21−28.

(19) Witten, T. A.; Leibler, L.; Pincus, P. A. *Macromolecules* **1990**, *23*, 824−829.
(20) Joanny, J. F. *Langmuir* **1992**, *8*, 989−995.
(21) Semenov, A. N. *Langmuir* **1995**, *11*, 3560−3564.
(22) Grest, G. S. *Curr. Opin. Colloid Interface Sci.* **1997**, *2*, 271−277.
(23) Kreer, T.; Muser, M. H.; Binder, K.; Klein, J. *Langmuir* **2001**, *17*, 7804−7813. Kreer, T.; Muser, M. H. *Wear* **2003**, *254*, 827−831. Neelov, I. M.; Borisov, O. V.; Binder, K. *J. Chem. Phys.* **1998**, *108*, 6973−6988. Joshi, Y. M.; Lele, A. K. *J. Rheol.* **2002**, *46*, 427−453.
(24) Taunton, H. J.; Toprakcioglu, C.; Fetters, L. J.; Klein, J. *Macromolecules* **1990**, *23*, 571−580.
(25) Widmaier, J. M.; Meyer, G. C. *Macromolecules* **1981**, *14*, 450−452.
(26) Hadjichristidis, N.; Xu, Z.; Fetters, L. J.; Roovers, J. *J. Polym. Sci., Polym. Phys. Ed.* **1982**, *20*, 743−750.
(27) Pearson, D. S.; Mueller, S. J.; Fetters, L. J.; Hadjichristidis, N. *J. Polym. Sci., Polym. Phys.* **1983**, *21*, 2287−2298.
(28) Brandrup, J., Immergut, E. H., Grulke, E. A., Eds. *Polymer Handbook*, 4th ed.; J. Wiley & Sons: New York, 1999.
(29) Klein, J.; Kumacheva, E. *J. Chem. Phys.* **1998**, *108*, 6996−7009.
(30) Tsarkova, L. A.; Protsenko, P. V.; Klein, J. *Colloid J.* (translation of *Kolloid. Zh.*) **2004**, *66*, 84−94.
(31) Ferry, J. D. *Viscoelastic Properties of Polymers*, 2nd ed.; John Wiley & Sons: New York, 1970.
(32) Georges, J.-M.; Tonck, A.; Loubet, J.-L.; Mazuyer, D.; Georges, E.; Sidoroff, F. *J. Phys. II* **1996**, *6*, 57−76.
(33) Mizuno, H.; Kjellin, M.; Nordgren, N.; Pettersson, T.; Wallqvist, V.; Fielden, M.; Rutland, M. W. *Aust. J. Chem.* **2006**, *59*, 390−393.
(34) Luengo, G.; Schmitt, F.-J.; Hill, R.; Israelachvili, J. *Macromolecules* **1997**, *30*, 2482−2494.
(35) Zhang, X.; Wilhelm, M.; Klein, J.; Pfaadt, M.; Meijer, E. W. *Langmuir* **2000**, *16*, 3884−3892.
(36) deGennes, P.-G. *Scaling Concepts in Polymer Physics*; Cornell University Press: Ithaca, NY, 1979.

MA062503G